https://doi.org/10.5194/egusphere-2026-4699
Preprint. Discussion started: 23 September 2026

Multi-Resolution Flood Hazard and Exposure Assessment in the Upper Narmada Basin

Pragya Badika[1], Nithila Devi Nallasamy[2], Nadja Veigel[2], Laurens J.N Oostwegel[3], Heidi Kreibich[2], Ankit Agarwal[1]

[1]Department of Hydrology, Indian Institute of Technology Roorkee, 247667, Uttarakhand, India

[2]Section 4.4: Hydrology, GFZ Helmholtz Centre for Geosciences, 14473 Potsdam, Germany

[3]Section 2.6, Seismic Hazard and Risk Dynamics, GFZ Helmholtz Centre for Geosciences, 14473 Potsdam, Germany

Correspondence to: Ankit Agarwal (Agarwal.10891.ankit@gmail.com/ ankit.agarwal@hy.iitr.ac.in)

https://doi.org/10.5194/egusphere-2026-4699
Preprint. Discussion started: 23 September 2026

Abstract

Spatial resolution strongly influences how flood hazards and exposed assets are represented, yet this source of uncertainty is often overlooked in impact-oriented flood studies. This study examines how hydraulic model resolution and exposure-data aggregation affect flood hazard classification and estimates of exposed buildings and population in the downstream reach of the Upper Narmada Basin, India. Two-dimensional flood simulations were performed for the August 2022 and 2020 events and evaluated using radar-derived inundation extent and observed discharge data. A 30 m hydraulic model was used as the reference and compared with coarser 140 m and 280 m resolutions. Building exposure was derived from combined OpenStreetMap and Open Buildings datasets, while population exposure was estimated using WorldPop data. Coarser resolutions systematically overestimated flood extent, hazard zones, and exposed elements. The overpredicted inundation area increased from 51.30 km^2 at 30 m to 58.45 km^2 at 140 m and 73.36 km^2 at 280 m. Similarly, the estimated number of affected buildings increased from 894 (2.5 times) at 30 m to 3051(8.8 times) at 140 m and 11 537 (33 times) at 280 m, while the affected population increased from 1612 to 5982 and 24 733, respectively. These results show that coarse-resolution hazard and exposure data can substantially inflate exposure estimates and may distort emergency planning, infrastructure prioritization, and resource allocation. Spatial resolution should therefore be treated as a key source of uncertainty in flood hazard and exposure assessment, and model/data resolution should be aligned with the research question and intended decision scale.

Keywords: Flood hazard assessment; exposure assessment; building exposure; population exposure; hydraulic model resolution; uncertainty propagation

https://doi.org/10.5194/egusphere-2026-4699
Preprint. Discussion started: 23 September 2026

1. Introduction

Floods are the most frequent, destructive and costliest worldwide (Guimarães Nobre et al., 2020) causing the largest average annualized losses globally compared to any other natural hazard (Williams et al., 2021). Flood directly affect lives, homes, livelihoods, crop production and hydraulic structures and regional economics. Globally, with 1.65 billion individuals affected, flooding accounts for the largest share of average annual disaster impacts (Alfieri et al., 2023). Riverine floods, one of the most common flood types, often cause severe damage to infrastructure and agriculture (Kimuli et al., 2021). Flooding is a devastating natural hazard in India, affecting approximately 21.21 million hectares leading to severe damage to agriculture, infrastructure, livelihoods, and human settlements (CWC, 2024). Between 1990 and 2022, floods affected over 629 million people, making India the second most flood-affected nation in terms of population with 46,000 fatalities and economic losses surpassing US$115 billion (Q. Liu et al., 2024), underscoring the country's high vulnerability to flooding.

The main drivers of increasing flood impacts include rapid population growth, expansion of settlements and investments in flood-prone areas, changes in upstream land-use patterns, and multi-day heavy precipitation (Pandidurai et al., 2026). Flooding is also likely to become more frequent and extensive in the future due to extreme weather events associated with a changing climate (Vogel et al., 2011). Rising temperatures driven by global climate change can intensify the severity and frequency of heavy precipitation events (Burn & Whitfield, 2023; Nithila Devi et al., 2025; Wasko et al., 2021; Wasko & Sharma, 2017)). Rapid urban growth further amplifies flooding by creating impervious surfaces, reducing infiltration, and increasing surface runoff (Huong & Pathirana, 2013; Nirupama & Simonovic, 2007; Olang & Fürst, 2011). Regions that fail to reduce exposure and vulnerability may therefore face serious consequences from increasing flood severity (Kreibich et al., 2017). These societal and environmental changes are expected to increase disaster impacts and costs, intensifying the need for effective reduction strategies (Arduino et al., 2005; Badika et al., 2024; Vashistha et al., 2025).

Understanding flood hazard, exposure, and potential impacts is essential for both society and the economy. Flood hazard and exposure assessment supports disaster preparedness, response, mitigation planning, and the protection of communities, infrastructure, and ecosystems. Such assessment combines different types of information and models to estimate flood extent, water depth, event characteristics, exposed elements, and potential consequences. In recent decades, flood assessment and management have gained increasing attention (Hooijer et al., 2004; Intergovernmental Panel on Climate Change (IPCC), 2023; Petrow et al., 2006). Flood maps are widely used to visualize hazard and exposure, support flood-management strategies, prioritize mitigation measures, and, in some countries, inform insurance-related decisions (De Bruijn & Klijn, 2009). A typical assessment begins with hazard analysis, which describes the likelihood and severity of possible flood events (Alfieri et al., 2013; Pappenberger et al., 2012). Hydrodynamic models are commonly used to simulate flood extent, water depth, and flow velocity, which provide the physical basis for impact calculations (Kiba et al., 2023). Exposure assessment then combines hazard maps with socio-economic information, such as building footprints, land-use maps, and population data, to translate physical flood characteristics into potential societal impacts (Jongman et al., 2012). Damage assessment can further link flood intensity with economic or human losses using vulnerability information (De Moel & Aerts, 2011; Kreibich & Thieken, 2008). However, translating modelling frameworks into reliable and usable flood-impact maps remains challenging.

Flood hazard and exposure mapping faces significant challenges due to the scarcity of accurate, high-resolution datasets, especially in data-scarce areas, and due to the trade-off between data detail and computational demand. Poor data quality can compromise hazard assessment and hinder effective communication of flood impacts (Merz et al., 2010; Schwanghart et al., 2024). Accurate flood modelling requires high-quality input data, including detailed digital elevation models (DEMs), land-cover information, and exposure datasets. However, using such detailed information increases computational time and processing requirements (Teng et al., 2017). In addition, uncertainties related to model structure, boundary conditions, parameters, and data scaling can affect the reliability of flood-impact estimates (Dasgupta et al., 2020; Ongdas et al., 2020; Rathod & Manekar, 2020). The present study focuses on the spatial resolution of the DEM and hydraulic model, as topography is an important factor for flood simulation accuracy. In this context, the spatial resolution of topographic data and hydraulic model grids is particularly important because topography strongly controls flood simulation accuracy (Altenau et al., 2017; Lim & Brandt, 2019; Sharma & Regonda, 2021a).

https://doi.org/10.5194/egusphere-2026-4699
Preprint. Discussion started: 23 September 2026

The DEM forms the foundation of hydraulic modelling, and its resolution determines how well important terrain features are represented. High-resolution DEMs can capture narrow channels, local drainage pathways, embankments, and small elevation differences, whereas coarse-resolution DEMs may oversimplify the landscape. In urban or complex rural environments, coarse models may miss narrow flow paths and produce artificial blockage effects, where terrain representation prevents water from following natural drainage pathways (Yu & Lane, 2006). The availability of high-resolution topographic data from remote sensing has improved flood modelling (Altenau et al., 2017; Sharma & Regonda, 2021a). But there is a nagging problem between precision and practicality. Moreover, in many regions, particularly in developing countries, generating or accessing very high-resolution DEMs over large areas remains difficult because of financial, logistical, and computational constraints (Y. Liu et al., 2025). Higher spatial resolution does not necessarily imply better accuracy, since it can add noise, increase computational cost, and require detailed parameterization. Therefore, identifying an appropriate or optimal resolution is an important research need. The selected resolution should be fine enough to represent key topographic features, such as narrow channels and local flow paths, while avoiding unnecessary computational burden (Azizian & Brocca, 2020; Brandt, 2016). If DEMs are too coarse, the landscape is oversimplified, resulting in artificial blockages or excessive smoothing that can distort flood pathways and inundation patterns (Yu & Lane, 2006).

This scale sensitivity is not limited to hazard modelling but also affects exposure assessment. Flood impacts vary strongly across space, and the representation of exposed buildings and population can influence final impact estimates. Building exposure may be assessed using individual building footprints or aggregated spatial units, such as census blocks or gridded exposure layers. The vulnerability and exposure of a building depend on its exact location, elevation, and relationship to the flood hazard. For example, impact estimates may differ depending on whether flood depth is evaluated at the building centre, across the entire building footprint, or within an aggregated exposure unit (Staffler et al., 2008; Zischg et al., 2018). Therefore, exposure assessment at multiple spatial scales is necessary to understand whether calculated impacts reflect actual exposure or are partly an artefact of spatial aggregation.

https://doi.org/10.5194/egusphere-2026-4699
Preprint. Discussion started: 23 September 2026

Although progress has been made in two-dimensional flood modelling and high-resolution data availability(Sharma & Regonda, 2021b; Vashist & Singh, 2023), important gaps remain in understanding how resolution-related uncertainty affects the flood hazard and exposure assessment chain. Previous studies have investigated the effect of DEM resolution on flood extent (Saksena & Merwade, 2015; Savage et al., 2016; Sharma & Regonda, 2021a) and the influence of hydraulic model resolution on loss-of-life estimation (Brussee et al., 2021). However, few studies have simultaneously evaluated the effects of hydraulic model resolution and exposure-map resolution (Bhere & Reddy, 2025) on flood impact assessment, particularly with respect to building and population exposure. To address this gap, the present study performs a multi-resolution flood hazard and exposure assessment for the flood-prone downstream region of the Upper Narmada Basin. The study systematically evaluates how spatial resolution influences flood inundation, hazard classification, building exposure, and population exposure. Specifically, it addresses the following research questions: how do changes in DEM resolution and hydraulic model grid size affect building-level and population exposure, and what resolution provides a practical balance between computational efficiency and reliable exposure mapping in the flood-prone area of the Upper Narmada Basin?

2. Study Area and data

The Narmada River is the largest westward flowing river in India. The Upper basin of the Narmada River covers an area of 42000 sq.km and is located between longitudes 72°38′–81°43′ E and latitudes 21°27′–23°37′ N (Fig. 1). At the downstream of the Upper Narmada basin, the Hoshangabad, Sehore and Raisen are more prone to the flood. The area of these districts has experienced numerous floods, in 1973, 1984, 1990, 2009, and 2013,2020,2022. Intense southwest monsoon rainfall is the primary cause of flooding in the upper catchment receives more than 1,400 mm of precipitation annually on average, with about 94% of that amount falling between June and October. During periods of intense rainfall, the upper basin's steep hilly and plateau terrain facilitates the effective routing of floodwaters into the main river channel and the quick formation of runoff. The upper basin has two major dams-Tawa and Bargi reservoir, and the basin has a general elevation of 600-900m.

https://doi.org/10.5194/egusphere-2026-4699
Preprint. Discussion started: 23 September 2026

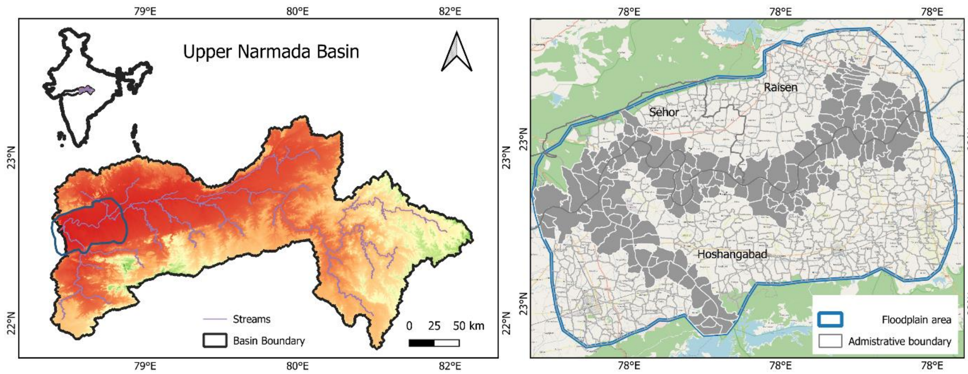

Figure 1: Location map of Upper Narmada Basin (left panel) along with the flood-prone area downstream of Upper Narmada Basin (right panel). (Credit: Basemap OSM Standard in QGIS)

We employed a digital elevation model of 30 m resolution of Shuttle Radar Terrain Model (SRTM) and resampled it to 140 m and 280 m resolution. For the setup of the hydrodynamic model, we chose 2022 and 2020 flood events at the downstream flood-prone area of the Upper Narmada Basin. For both flood events 2022 and 2020, the flood hydrograph of Sandia and Hoshangabad collected from the India WRIS, and the flood hydrograph of the Tawa is collected from the daily reports generated by the Narmada Control Authority. The number of buildings exposed to flooding was obtained from a conflation of OpenStreetMap buildings (refer www.openstreetmap.org) and the Open Building dataset (Sirko et al., 2021) adapted from **(Schorlemmer et al., 2024)**. Occupancy type (residential, commercial and industries) was estimated using land use areas and points of interest (e.g. restaurants, schools or hotels) from Open Street Map and attributes from the buildings (e.g. footprint area). The estimation of the population exposed to flooding was estimated using the WorldPop data (Bondarenko et al., 2020). The building and population exposure available at individual building level and aggregated to 140 m and 280 m resolution. The attributes of administrative village data are collected from the Survey of India.

3. Methods

The workflow to assess building and population exposure in the flood-prone area of the Upper Narmada Basin is shown in Fig. 2. It employs a hydraulic modelling framework for

https://doi.org/10.5194/egusphere-2026-4699
Preprint. Discussion started: 23 September 2026

hazard assessment, followed by building and population exposure assessment at different spatial resolutions. This section describes the data, model setup, and methods used for flood hazard and exposure analysis.

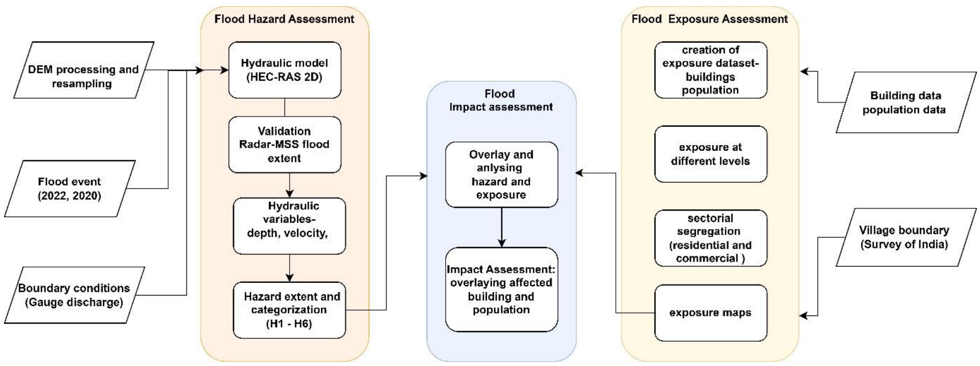

Figure 2: Methodological framework for multi-resolution flood hazard and exposure assessment.

3.1 Resolutions

In the exposure dataset, the building entities are organized using the Quad tree grid (Finkel & Bentley, 1974), with the Quad tiles projected using the Web Mercator projection (EPSG:3857). The the Quad tiles are organized at zoom level 18, which roughly translates to 140 x 140 m in the case study area.

Based on the availability of exposure data, three spatial resolutions are considered:

1. Resolution 30 m: the 30 m DEM and hydraulic model grid are used for hazard assessment, and individual building footprints are used for exposure assessment.
2. Resolution 140 m: exposure entities are represented by 140 × 140 m tiles (zoom level 18), and the DEM and hydraulic model grid are resampled to 140 m.
3. Resolution 280 m: exposure entities are represented by 280 × 280 m tiles (zoom level 17), and the DEM and hydraulic model grid are resampled to 280 m.

3.2 Flood Hazard Simulation

The study employs a hydraulic model to simulate the 2022 and 2020 flood events. The hydraulic domain covers the downstream districts of Hoshangabad, Sehore, and Raisen in the Upper Narmada Basin. The model uses SRTM DEM data with an original spatial

https://doi.org/10.5194/egusphere-2026-4699
Preprint. Discussion started: 23 September 2026

resolution of 30 m, which was also resampled to 140 m and 280 m. The two-dimensional Hydrologic Engineering Centre–River Analysis System version 6.4.1 (HEC-RAS) (USACE, 2016) is used to route upstream discharge through the hydraulic domain. The upstream boundary conditions are defined at Sandia on the main Narmada River and at Tawa on a major tributary, while the downstream boundary is located near the Hoshangabad gauging station. A reference line at Hoshangabad gauging station is used to verify the simulated hydrograph. The upstream hydrographs at Sandia and Tawa were obtained from India-WRIS and the Narmada Control Authority, respectively, for both flood events and all three resolutions. For the 2022 flood, cloud-free radar/MSS-derived inundation extent and river-flow observations at Hoshangabad were available for model validation. To avoid over-parameterization and equifinality, a uniform Manning's roughness was used for the floodplain, which is justified by the relatively uniform land use in the simulation domain. A sensitivity analysis was conducted using nine combinations of channel and floodplain Manning's roughness values, and model performance was evaluated using the fitness index for inundation extent, NSE, and RRMSE of the flood hydrograph. The validated hydraulic model provides flood depth, velocity, and inundation extent for the subsequent hazard and exposure analysis. The analysis is limited to the hydraulic domain covering the three downstream districts.

3.3 Flood Hazard Zones

Flood hazard characteristics, namely flood depth and velocity, are categorized using vulnerability thresholds for exposed people, buildings, and vehicles (Supplementary Tables S1 and S2). Six hazard zones (H1 to H6) represent progressively increasing threats to inhabitants and assets. H1 is generally safe for people, vehicles, and buildings; H2 is unsafe for small vehicles; H3 is unsafe for vehicles, children, and the elderly; H4 is unsafe for people in general; H5 indicates conditions under which buildings are vulnerable to structural damage; and H6 indicates conditions under which buildings may fail. For the three spatial resolutions, we estimate exposed buildings and population across these hazard classes.

3.4 Exposure Assessment

The number of buildings exposed to flooding was obtained from a conflation of OpenStreetMap buildings (OpenStreetMap, 2024) and the Open Building dataset (Sirko

https://doi.org/10.5194/egusphere-2026-4699
Preprint. Discussion started: 23 September 2026

et al., 2021) adapted from (Schorlemmer et al., 2024). Occupancy type-residential, commercial or industrial were estimated to use land use areas and points of interest (e.g. restaurants, schools or hotels) from Open Street Map and attributes from the buildings (e.g. footprint area). The population exposure for residential and commercial buildings were estimated by WorldPop data (Bondarenko et al., 2020). The building and population exposure are available at individual building (z-level) and these are further aggregated at two levels-Z17 and Z18. In Z17 level, the buildings are aggregated at the spatial resolution of 280 × 280 m, and Z18 level is aggregated at the spatial resolution of 140 × 140 m. All three levels have separate residential, commercial, and industrial taxonomy. These taxonomies provide the buildings assets like number of buildings, number of populations at night and the structural value. In our current study, we used the building and population in two sectors- residential sector and commercial sector (commercial plus industrial buildings) for all three resolutions.

4. Results

4.1 Flood inundation mapping/ Hydraulic modelling

The calibration and validation results of the hydraulic modelling for flood inundation mapping are presented in this section. For each model resolution, nine combinations of Manning's roughness coefficients were tested for the channel and floodplain, and the best-performing combination was selected based on the fitness index, Nash–Sutcliffe efficiency (NSE), and relative root mean square error (RRMSE), as shown in Table 1. The results indicate that changing channel roughness has a stronger influence on model performance than changing floodplain roughness. This is physically meaningful because channel roughness directly controls flow conveyance, flood-wave propagation, water level, and downstream discharge, whereas floodplain roughness mainly influences lateral spreading and storage after overbank flow occurs.

As shown in Table 1, the best-performing Manning's roughness coefficients for the 30 × 30 m resolution were 0.02 for the channel and 0.03 for the floodplain. The same values were also found suitable for the 140 × 140 m resolution. For the 280 × 280 m resolution, the best-performing coefficients were 0.02 for the channel and 0.09 for the floodplain. This variation reflects the influence of grid resolution on the representation of terrain and surface heterogeneity. Finer-resolution models, such as 30 × 30 m, capture channel

https://doi.org/10.5194/egusphere-2026-4699
Preprint. Discussion started: 23 September 2026

geometry, local topographic gradients, drainage pathways, and floodplain features more effectively, and therefore require lower and more physically realistic roughness values. In contrast, coarser models, such as 280 × 280 m, smooth terrain and vegetation details, reduce the representation of local barriers and depressions, and therefore require higher effective floodplain roughness to reproduce the observed flood dynamics.

Table 1: Hydraulic model performance for the 2022 flood event at 30 × 30 m, 140 × 140 m, and 280 × 280 m spatial resolutions under different channel and floodplain Manning's roughness combinations. Model performance is evaluated using the fitness index for inundation extent, Nash–Sutcliffe efficiency (NSE), and relative root mean square error (RRMSE), with the optimal parameter set identified for each resolution.

	Fitness Index				**NSE**				**RRMSE**		
					30 x 30m Resolution						
	n_floodplain				n_floodplain				n_floodplain		
n_channel	**0.03**	**0.06**	**0.09**	n_channel	**0.03**	**0.06**	**0.09**	n_channel	**0.03**	**0.06**	**0.09**
0.02	0.60	0.60	0.60	**0.02**	0.91	0.91	0.91	**0.02**	0.21	0.32	0.33
0.03	0.51	0.50	0.50	**0.03**	0.84	0.83	0.82	**0.03**	0.31	0.32	0.33
0.04	0.46	0.46	0.42	**0.04**	0.7	0.67	0.32	**0.04**	0.42	0.44	0.64
					140 x 140m resolution						
	n_floodplain				n_floodplain				n_floodplain		
n_channel	**0.03**	**0.06**	**0.09**	n_channel	**0.03**	**0.06**	**0.09**	n_channel	**0.03**	**0.06**	**0.09**
0.02	0.54	0.54	0.54	**0.02**	0.9	0.89	0.89	**0.02**	0.25	0.25	0.25
0.03	0.47	0.47	0.41	**0.03**	0.81	0.78	0.33	**0.03**	0.34	0.36	0.64
0.04	0.44	0.44	0.44	**0.04**	0.69	0.62	0.59	**0.04**	0.43	0.48	0.50
					280 x 280m resolution						
	n_floodplain				n_floodplain				n_floodplain		
n_channel	**0.03**	**0.06**	**0.09**	n_channel	**0.03**	**0.06**	**0.09**	n_channel	**0.03**	**0.06**	**0.09**
0.02	0.45	0.44	0.54	**0.02**	0.86	0.83	0.89	**0.02**	0.29	0.32	0.25
0.03	0.43	0.42	0.42	**0.03**	0.74	0.65	0.59	**0.03**	0.39	0.46	0.50
0.04	0.42	0.41	0.41	**0.04**	0.64	0.5	0.42	**0.04**	0.47	0.55	0.59

The validation of the selected parameter combinations is shown in Fig. 3, where the simulated maximum flood inundation extents are compared with the radar- and MSS-

https://doi.org/10.5194/egusphere-2026-4699
Preprint. Discussion started: 23 September 2026

derived flood extent. The 30 × 30 m model captures the observed inundation pattern most effectively, indicating that the finer grid better represents the main flow paths and floodplain connectivity. As the grid resolution becomes coarser from 30 × 30 m to 140 × 140 m and 280 × 280 m, the model increasingly overpredicts the inundated area. The overpredicted area is 51.30 km^2 for the 30 × 30 m model, 58.45 km^2 for the 140 × 140 m model, and 73.36 km^2 for the 280 × 280 m model. Thus, compared with the 30 × 30 m model, overprediction increases by about 13.9% for the 140 × 140 m model and by about 43% for the 280 × 280 m model. This increase occurs because coarse grids average elevation over larger cells, smooth small topographic barriers, and reduce the representation of narrow drainage pathways, allowing water to spread more widely across the floodplain.

The model was also validated for the 2020 flood event, and the corresponding performance indices are reported in Supplementary Table S3. The NSE and RRMSE values are within an acceptable range, confirming that the model can reproduce the general flood response. However, the 30 × 30 m resolution again performs better than the 140 × 140 m and 280 × 280 m resolutions. Although the broad inundation pattern is similar across all three resolutions, important differences are observed near riverbank villages, where local topography strongly controls flood depth, velocity, and lateral spreading. These results demonstrate that model resolution has a strong influence not only on total inundated area but also on the spatial distribution of flood characteristics, which directly affects subsequent hazard classification and exposure assessment.

https://doi.org/10.5194/egusphere-2026-4699
Preprint. Discussion started: 23 September 2026

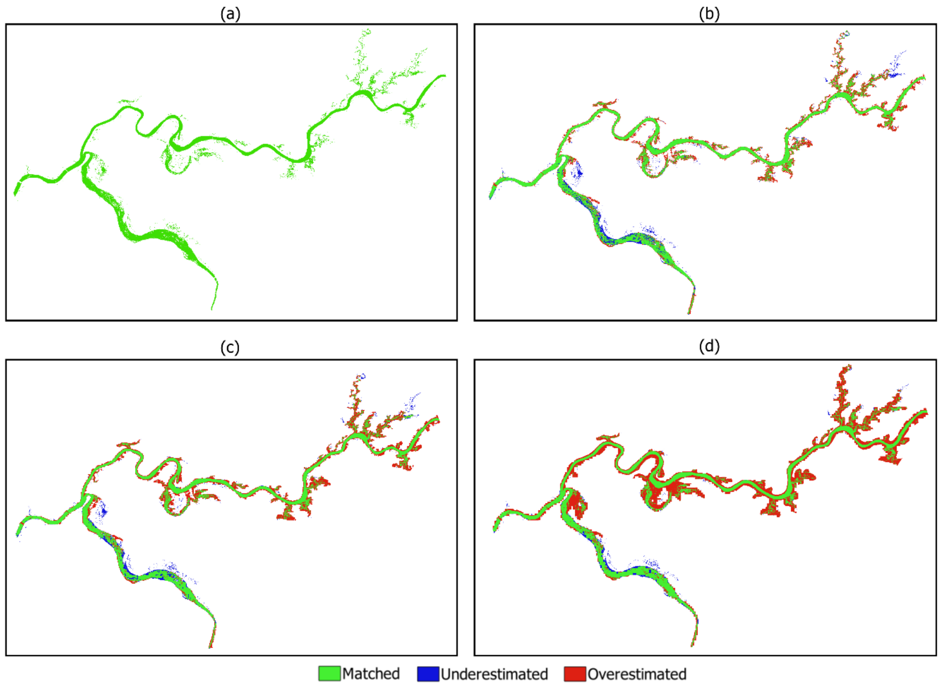

Figure 3: Comparison of the maximum inundation extents simulated by HEC-RAS 2D at spatial resolution (b)30 × 30 m, (c)140 × 140 m, (d)280 × 280 m, with the (a) observed inundation extent derived from Radar and MSS.

4.2 **Flood Hazard**

Figure 4 illustrates the effect of spatial resolution on flood hazard mapping using HEC-RAS 2D. By comparing the 30 × 30 m baseline with the coarser 140 × 140 m and 280 × 280 m resolution simulations, it is evident that coarsening the grid reduces the model's ability to represent terrain accurately and therefore affects both the extent and classification of flood hazard. The 30 m model captures the micro-topography of the landscape more effectively, including narrow drainage channels, small levees, and subtle elevation variations, which control where water flows, accumulates, and remains confined. As resolution becomes coarser, these features are progressively smoothed or lost. This effect is clearly visible in the zoomed panels of Fig. 4, where the hazard zones change from relatively continuous and spatially detailed patterns at 30 m to more blocky and generalized clusters at 140 m and especially at 280 m.

https://doi.org/10.5194/egusphere-2026-4699
Preprint. Discussion started: 23 September 2026

The physical reason for this behavior is that coarse grid cells average elevation over larger areas cannot distinguish narrow streams, local depressions, or small dry patches adjacent to inundated zones. As a result, water that is confined to limited pathways in the 30 m model spreads over broader areas in the 140 m and 280 m models. If part of a large grid cell is inundated, the whole cell may be classified as flooded, which artificially inflates the mapped hazard extent. This causes neighboring tributaries and floodplain patches to merge into larger continuous hazard zones, particularly in the 280 m simulation.

Figure 4(d) quantifies these effects through the relative change in area under each hazard category (H1–H6) for the 140 × 140 m and 280 × 280 m resolution compared with the 30 × 30 m baseline resolution. For all hazard classes, the area difference is positive, indicating that the coarse-resolution models consistently overestimate the hazard footprint. The effect is strongest for the 280 m model, especially for Hazard Zone H5, where the estimated area is about 150% higher than in the 30 m simulation. In other words, the 280 m model predicts more than twice the area under high hazard conditions compared with the finer-resolution baseline. Even the 140 m model shows systematic increases, generally ranging from about 10% to 40% across the hazard classes.

In addition to changing the hazard extent, coarsening the grid also affects hazard classification. Because hazard zones are derived from a combination of flood depth and flow velocity, any smoothing of topography alters the distribution of these hydraulic variables. In coarse-resolution models, the terrain becomes flatter in an effective sense, which allows water to spread laterally over a larger area with more uniform depth and lower spatial variability. Instead of being concentrated within deeper and more confined flow paths, floodwater is redistributed into broader and shallower cells. This redistribution can shift areas from one hazard class to another, as reflected in the H5 and H6 patterns in Fig. 4. Although coarser grids such as 280 m reduce computational demand, they do so at the cost of substantial loss of spatial precision. Using such coarse-resolution outputs for flood hazard planning may therefore lead to inflated hazard estimates and overly conservative or misdirected mitigation decisions.

https://doi.org/10.5194/egusphere-2026-4699
Preprint. Discussion started: 23 September 2026

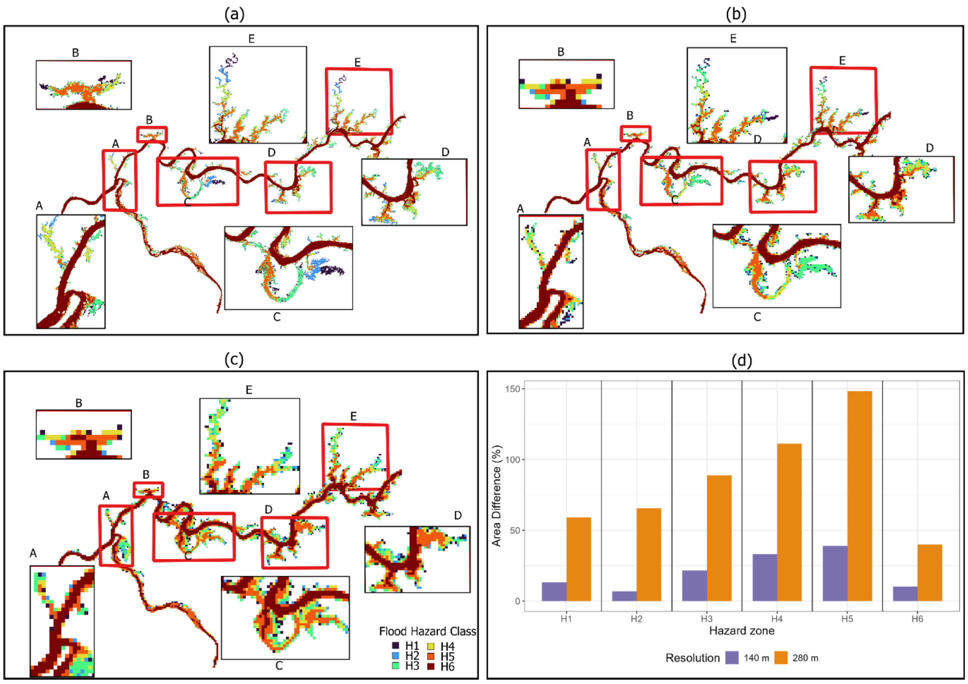

Figure 4: Maximum flood hazard extent simulated by HEC-RAS 2D at spatial resolutions of (a) 30 × 30 m, (b) 140 × 140 m, and (c) 280 × 280 m. Panel (d) shows the relative change in area under each flood hazard category (H1–H6) for the 140 × 140 m and 280 × 280 m resolutions with respect to the 30 × 30 m resolution. Zoomed views of the hazard zones are also shown for the three grid resolutions to illustrate the effect of spatial resolution on the spatial distribution and classification of flood hazard.

4.3 Exposure of people and buildings at different resolutions

To assess how model resolution influences flood exposure, the 140 × 140 m and 280 × 280 m resolutions were compared with the 30 × 30 m baseline. Fig. 5 presents the transition matrix of affected buildings and population across flood hazard categories. Each bubble represents the number of buildings and exposed population that shift from one hazard class in the 30 × 30 m baseline to another hazard class in the coarser resolutions. For example, a bubble located at H3 on the baseline axis and H4 on the coarser-resolution axis indicates that buildings or people classified under H3 at 30 m are reclassified as H4 after spatial aggregation. Bubbles along the 1:1 line indicate no change in hazard classification, whereas bubbles above the line represent an increase in hazard class and bubbles below the line represent a decrease. In the 140 × 140 m resolution, most bubbles remain close to the 1:1 line, indicating that a large proportion of buildings and population retain the same hazard classification as in the 30 × 30 m baseline. This suggests that, although some aggregation effects are present at 140 × 140 m, the exposure pattern remains relatively consistent with the finer-resolution model.

In contrast, the 280 × 280 m resolution shows much larger off-diagonal transitions, indicating stronger deviation from the 30 × 30 m baseline. A notable feature in both coarser resolutions is the redistribution of buildings and population originally classified as H0* in the baseline into hazard classes H1–H6. This means that areas considered non-flooded in the 30 × 30 m simulation become classified as flooded when the hazard and exposure layers are represented at coarser resolutions. Physically, this occurs because coarse grids smooth local topographic controls and expand the simulated flood footprint, thereby assigning flood hazard to areas that remain dry in the finer-resolution model.

The wider scatter of bubbles away from the 1:1 line in the 280 × 280 m matrix shows that coarser resolution substantially alters the representation of flood exposure across hazard classes. Some transitions from higher to lower hazard categories are also observed, indicating localized reductions in estimated hazard severity. However, these downward transitions are mostly limited to adjacent hazard classes and are smaller in magnitude than the dominant diagonal and upward transitions.

The 140 × 140 m resolution exposes 1,314 buildings and 2,634 people to flooding, mainly from unaffected areas (H0*), particularly in transitions to H5 and H6, which account for over 70% of new exposures. The 280 × 280 m resolution increases this to 9,155 buildings and 20,461 people, with major transitions also from H0 to H5 and H6. This shows a marked rise in high-hazard class exposure and a reduction in unaffected assets, indicating both greater flood extent and intensified severity. Marginal bar plots reveal a shift in flood exposure from the unaffected class (H0) to higher hazard classes as resolution changes. In the 140 × 140 m resolution, unaffected assets drop from 3,031 to 268 people and from 1,536 to 157 buildings, while H6 and H5 show significant concentration. The 280 × 280 m resolution further reduces unaffected numbers to 172 people and 125 buildings, while H5–H6 exposure increases to 12,275 people and 5,286 buildings, over four times more than at 140 m. This shift indicates a critical increase in flood exposure towards the most

https://doi.org/10.5194/egusphere-2026-4699
Preprint. Discussion started: 23 September 2026

hazardous classes with coarser resolution. Fig. 5 shows that coarser model resolution not only increases the number of exposed buildings and population but also changes their distribution among hazard classes, which can directly influence impact interpretation and emergency-planning priorities.

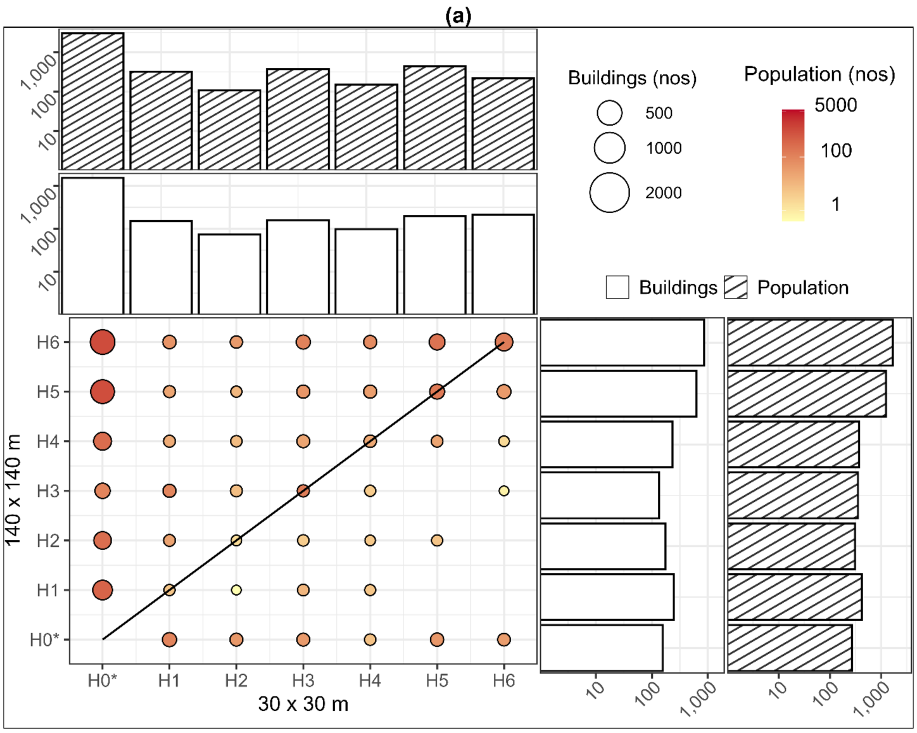

404

https://doi.org/10.5194/egusphere-2026-4699
Preprint. Discussion started: 23 September 2026

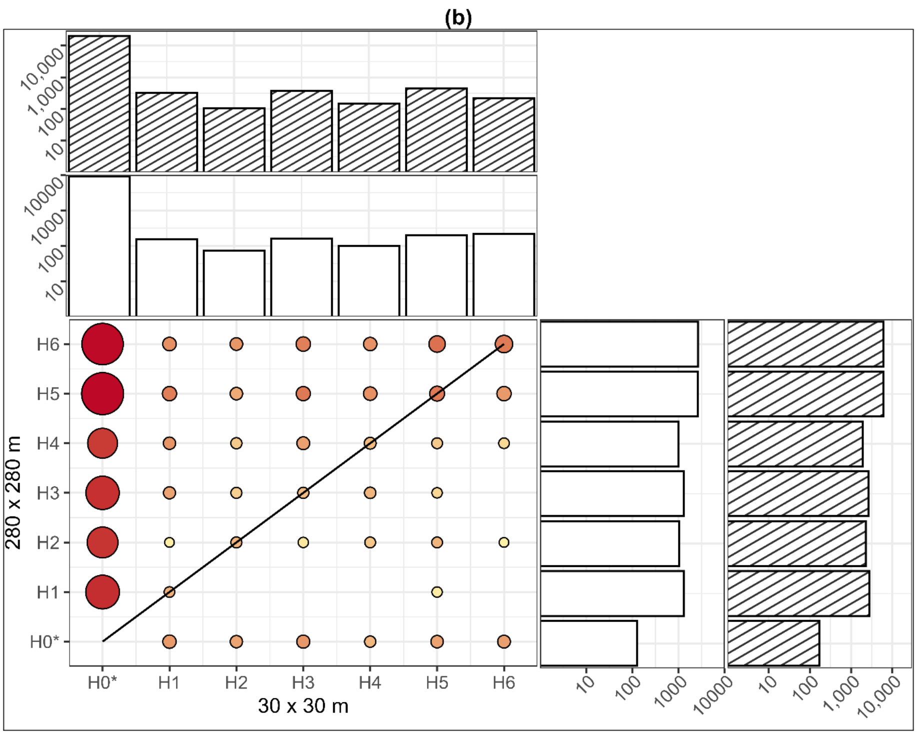

Figure 5: Flood exposure transition matrix comparing the 30 × 30 m resolution with the coarser resolutions of (a) 140 × 140 m and (b) 280 × 280 m. H0* represents the non-flooded class. Each bubble indicates the transition of exposed buildings and population from one hazard class in the 30 x 30 m resolution to another hazard class in the coarser resolution. Bubble size represents the number of affected buildings, while bubble color represents the exposed population.

4.4 Affected exposure patterns at different spatial resolutions

The quantitative differences among the resolutions are summarized in Table 2 and Fig. 6d. The number of affected buildings and exposed population increases markedly as the spatial resolution becomes coarser. Total affected buildings increase from 346 in the satellite-derived reference to 894 in the 30 × 30 m resolution, 3051 in the 140 × 140 m resolution, and 11 537 in the 280 × 280 m resolution. Similarly, the affected population increases from 550 in the satellite reference to 1612, 5982, and 24 733 in the 30 m, 140 m, and 280 m resolution, respectively. This sharp increase shows that exposure estimates

https://doi.org/10.5194/egusphere-2026-4699
Preprint. Discussion started: 23 September 2026

are strongly controlled by the spatial resolution at which flood hazard and assets are represented.

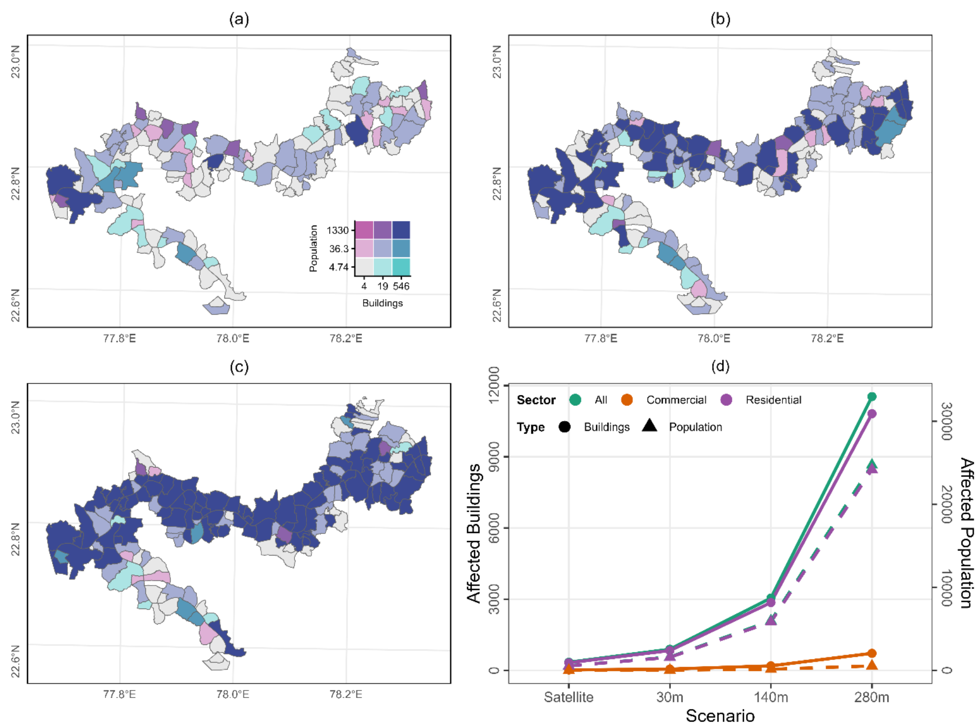

Figure 6: Village-level distribution of affected buildings and exposed population under the (a) 30 × 30 m, (b) 140 × 140 m, and (c) 280 × 280 m resolutions. Panel (d) compares the number of affected buildings and exposed population across all buildings, residential buildings, and commercial buildings for each spatial resolution. Circles represent affected buildings, while triangles represent exposed population.

The sectoral results in Table 2 further show that residential exposure dominates the total affected buildings and population across all resolutions. Residential buildings increase from 837 at 30 × 30 m to 10 816 at 280 × 280 m, while the affected residential population increases from 1577 to 24 190. Commercial exposure also increases with coarser resolution, from 57 affected buildings at 30 × 30 m to 721 at 280 × 280 m. Although commercial buildings represent a smaller share of the total exposed structures, their inclusion is important because they may carry higher economic value and contribute to

https://doi.org/10.5194/egusphere-2026-4699
Preprint. Discussion started: 23 September 2026

indirect flood losses. The increase in both residential and commercial exposure at coarser scales indicates that the 280 m model assigns flood hazard to many assets that remain outside the inundated area in the finer-resolution simulation.

Table 2: Number of affected buildings and exposed population under the satellite-derived reference, 30 × 30 m, 140 × 140 m, and 280 × 280 m resolutions. Results are presented for all buildings and population, residential buildings and population, and commercial buildings and population to show how exposure estimates vary across sectors and spatial resolutions.

All buildings & population				
	Satellite	**Model_30m**	**Model_140m**	**Model_280m**
Building	346	894	3051	11537
Population	550	1612	5982	24733
Residential buildings & population				
	satellite	**Model_30m**	**Model_140m**	**Model_280m**
Building	324	837	2859	10816
Population	538	1577	5839	24190
Commercial buildings & population				
	satellite	**Model_30m**	**Model_140m**	**Model_280m**
Building	22	57	193	721
Population	12	35	143	543

Fig. 7 further illustrates the distribution of affected buildings and population across villages. The histograms show a strongly right-skewed pattern in all resolutions, meaning that most villages experience relatively low impacts, while a small number of villages account for very high exposure. In the satellite and 30 × 30 m resolution, most villages remain in the lower-impact classes. However, as the resolution becomes coarser, the distribution shifts toward larger values, with more villages showing high numbers of affected buildings and population. The 280 × 280 m resolution produces the widest distribution and the largest extreme values, with some villages showing more than 600 affected buildings and population exposure approaching 2000 people.

https://doi.org/10.5194/egusphere-2026-4699
Preprint. Discussion started: 23 September 2026

Fig. 6, Table 2, and Fig. 7 demonstrate that coarser-resolution modelling can substantially inflate village-level exposure estimates. This does not necessarily indicate a real increase in impact but rather reflects the combined effects of expanded flood footprints, spatial aggregation, and loss of local topographic detail. Such overestimation may distort the identification of exposure hotspots and affect emergency planning, mitigation prioritization, and resource allocation. Therefore, high-resolution hazard and exposure data are particularly important when flood hazard and exposure information is used for local-scale decision-making.

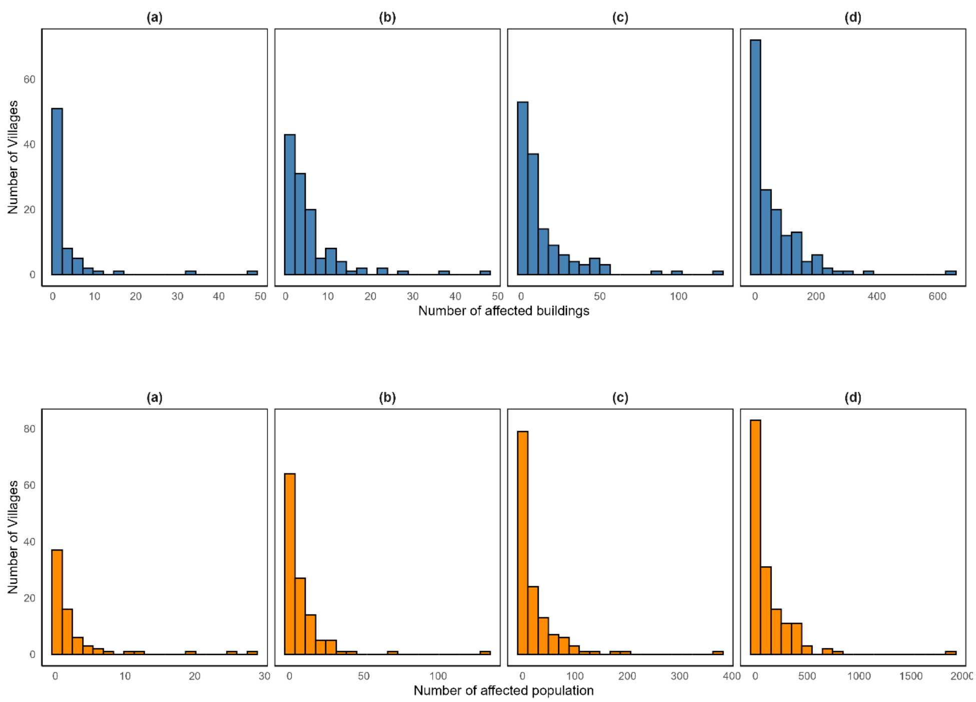

Figure 7: Frequency distribution of affected buildings (upper panel) and exposed population (lower panel) across villages under the (a) satellite-derived reference, (b) 30 × 30 m, (c) 140 × 140 m, and (d) 280 × 280 m resolutions. The top row shows the distribution of affected buildings, while the bottom row shows the distribution of exposed population.

https://doi.org/10.5194/egusphere-2026-4699
Preprint. Discussion started: 23 September 2026

5. Discussion

5.1 Resolution effects on flood hazard simulation

Our results demonstrate that spatial resolution is a key control on the accuracy and interpretation of flood hazard simulation. The comparison of the 30 × 30 m, 140 × 140 m, and 280 × 280 m HEC-RAS 2D simulations shows that coarser model grids systematically overestimate flood extent and modify the spatial distribution of flood hazard classes. This behaviour is consistent with previous studies showing that DEM and hydraulic grid resolution strongly influence flood inundation modelling by controlling how channels, floodplain gradients, embankments, depressions, and local flow pathways are represented (Brussee et al., 2021; Fewtrell et al., 2008; Jiang et al., 2022; Saksena & Merwade, 2015; Savage et al., 2016; Yu & Lane, 2006).

The calibration results in Table 1 show that channel roughness has a stronger effect on model performance than floodplain roughness. This is physically meaningful because the main channel controls flow conveyance, water-level propagation, and downstream discharge, whereas floodplain roughness mainly influences lateral spreading and temporary storage after overbank flow begins. The best-performing roughness values also vary with resolution, especially for the floodplain. The 30 × 30 m and 140 × 140 m simulations perform well with lower floodplain roughness, whereas the 280 × 280 m simulation requires a higher effective floodplain roughness. This indicates that coarse grids compensate for the loss of unresolved floodplain features, such as small terrain barriers, vegetation heterogeneity, depressions, and local drainage pathways, through an adjusted roughness parameter.

The validation against radar- and MSS-derived inundation extent in Fig. 3 further confirms that the 30 × 30 m model provides the most reliable representation of the observed flood pattern. As grid size increases, elevation values are averaged over larger cells, which smooths local topographic controls and allows water to spread over broader floodplain areas. Consequently, the overpredicted inundation area increases from 51.30 km^2 at 30 m to 58.45 km^2 at 140 m and 73.36 km^2 at 280 m. The 2020 validation results reported in Supplementary Table S2 also indicate acceptable model performance but again show better performance for the 30 × 30 m resolution than for the coarser resolutions. This consistency across events strengthens the interpretation that the

https://doi.org/10.5194/egusphere-2026-4699
Preprint. Discussion started: 23 September 2026

observed differences are not only event-specific but are linked to spatial representation in the model.

The effect of resolution becomes more evident in the flood hazard classification shown in Fig. 4. Hazard classes are derived from flood depth and velocity, and both variables are sensitive to how terrain and flow pathways are represented. At 30 m resolution, the model preserves relatively continuous and physically realistic flood pathways. In contrast, the 140 m and especially the 280 m simulations produce more generalized, blocky hazard zones. Figure 4(d) shows that all hazard classes increase in area under coarser resolutions, with the strongest increase in high-hazard zones such as H5. This suggests that coarse-resolution modelling does not simply change the total flood extent; it also redistributes depth and velocity patterns, thereby altering the classification of flood severity. These results emphasize that hazard maps should not be interpreted as purely physical outputs independent of scale. Rather, they are strongly shaped by the spatial resolution of the terrain and hydraulic model.

5.2 Propagation of resolution uncertainty into exposure estimates

A major contribution of this study is that it evaluates how resolution-induced differences in flood hazard propagate into building and population exposure estimates. Impact-oriented flood studies are generally built on linked components: hazard, exposure, and vulnerability or impact estimation (Alfieri et al., 2013; Jongman et al., 2012; Pappenberger et al., 2012). Uncertainties introduced during hazard modelling can therefore directly influence the number of buildings and people classified as exposed. This study shows that such propagation is substantial when both hazard and exposure are represented at coarser spatial resolutions.

The transition matrices in Fig. 5 provide clear evidence of this propagation. In the 140 × 140 m resolution, many exposed elements remain close to the 1:1 line, indicating that their hazard classification is similar to the 30 × 30 m baseline. In the 280 × 280 m resolution, the larger number of off-diagonal transitions shows that coarser resolution substantially changes the assignment of buildings and population to hazard classes. A particularly important result is the movement of buildings and people from H0*, the non-flooded class in the 30 m baseline, into flooded hazard classes H1–H6 under coarser resolutions. This means that assets considered safe in the finer-resolution model are classified as exposed when the hazard and exposure layers are aggregated. Physically,

https://doi.org/10.5194/egusphere-2026-4699
Preprint. Discussion started: 23 September 2026

this occurs because the coarser grid expands the inundation footprint and assigns flood conditions to larger spatial units, even where local topographic features would keep some areas dry.

The sectoral exposure estimates in Table 2 and the village-level patterns in Fig. 6 show the magnitude of this effect. The number of affected buildings increases from 894 at 30 m to 3051 at 140 m and 11 537 at 280 m, while the affected population increases from 1612 to 5982 and 24 733, respectively. Residential exposure dominates the total affected buildings and population across all resolutions, which is expected because population distribution is closely linked to residential structures. Commercial exposure is smaller in absolute numbers but remains important because commercial and industrial assets may represent higher economic value and can contribute to indirect losses through disruption of local services and livelihoods.

The bivariate maps in Fig. 6 show that high-exposure villages are concentrated mainly in the central and eastern parts of the study domain, while the western and southern margins show lower exposure. This spatial pattern suggests that flood impact is controlled by both physical floodplain characteristics and the distribution of settlements and built assets. As the grid becomes coarser, high-exposure zones expand spatially and more villages are classified as affected. This does not necessarily indicate a real increase in flood impact; it reflects the combined effect of a broader simulated flood footprint and the aggregation of exposure data.

Figure 7 further supports this interpretation by showing the frequency distribution of affected buildings and exposed population across villages. In all resolutions, the distributions are strongly right skewed, meaning that most villages experience relatively low exposure while a small number of villages account for very high impacts. The 280 × 280 m resolution produces the widest distribution and the largest extreme values, with some villages showing more than 600 affected buildings and population exposure approaching 2000 people. This indicates that coarse-resolution modelling can exaggerate village-level exposure hotspots and may shift attention toward locations where exposure is partly an artefact of spatial aggregation.

These findings show that exposure estimates are affected not only by the physical hazard but also by the scale at which exposure is represented. Similar concerns have been raised in flood damage and exposure studies, where uncertainties in inundation depth, exposure data, asset values, and vulnerability functions can strongly affect final impact estimates

https://doi.org/10.5194/egusphere-2026-4699
Preprint. Discussion started: 23 September 2026

(De Moel & Aerts, 2011; Jongman et al., 2012; Kreibich et al., 2017). The present study extends this understanding by demonstrating that the interaction between hydraulic model resolution and exposure-map resolution can strongly influence building- and population-level exposure indicators. Therefore, hazard and exposure resolution should be assessed together, rather than treated as independent sources of uncertainty.

5.3 Implications for flood hazard and exposure mapping and decision-making

The findings have direct implications for flood hazard and exposure mapping, as well as for model-scale selection. High-resolution simulations provide a more realistic representation of local flood processes, but they require greater computational resources and detailed input data. Coarser simulations are computationally attractive for large-area assessments, but they can introduce substantial bias in inundation extent, hazard classification, and exposure estimates. This trade-off has been widely recognized in flood modelling studies (Bates, 2012; Teng et al., 2017), and the present results show that it becomes especially important when flood maps are used for impact-based decision-making.

For regional screening, coarser-resolution models may still be useful for identifying broad flood-prone corridors and prioritizing areas for further analysis. However, the results suggest that coarse-resolution outputs, especially at 280 m, should be used cautiously for local-scale planning. If such outputs are used directly for evacuation planning, village-level prioritization, infrastructure protection, or resource allocation, they may overestimate the number of affected buildings and people. This could lead to overly conservative planning in some areas, misallocation of resources, and reduced confidence in hazard and exposure products. High-resolution hazard and exposure data are more appropriate when the objective is to identify local hotspots, assess building-level exposure, or support targeted mitigation measures.

The results also have implications for data-scarce regions. In many developing-country contexts, very high-resolution DEMs and detailed exposure datasets may not be available or may be too costly to process over large areas. In such settings, the objective should not always be to use the finest possible resolution, but to select a resolution that is consistent with the intended decision scale. The 30 m resolution in this study provides a more reliable baseline for building and population exposure assessment than the 140 m and 280 m resolutions. Moderate-resolution products may still be useful for preliminary

https://doi.org/10.5194/egusphere-2026-4699
Preprint. Discussion started: 23 September 2026

assessments if their uncertainty is clearly communicated and if they are not used for highly localized decisions without further refinement.

This study also highlights the need to communicate uncertainty in flood hazard and exposure maps. Flood maps are often treated as deterministic products, but the results show that changes in resolution alone can strongly alter the number of affected buildings, exposed population, and apparent exposure hotspots. Decision-makers should therefore interpret flood maps as scale-dependent estimates rather than fixed representations of reality. For practical applications, model outputs should ideally be accompanied by information on spatial resolution, input data limitations, validation performance, and uncertainty in exposure estimates.

Some limitations should also be acknowledged. The study focuses on flood hazard and exposure indicators and does not quantify direct economic damages, structural damage probabilities, or loss of life using vulnerability or damage functions. Therefore, the results should be interpreted as exposure-based impact estimates rather than complete damage or loss estimates. Future work should integrate depth-damage curves, building vulnerability functions, observed damage records, and uncertainty analysis across multiple flood events. Application of the framework to other river basins and to higher-resolution topographic and exposure datasets would further help identify transferable scale thresholds for reliable flood hazard and exposure mapping.

Spatial resolution is not a technical modelling detail but a central source of uncertainty in flood hazard and exposure assessment. The resolution of hazard and exposure datasets must be aligned with the intended use of the map. For broad regional screening, coarser models may be acceptable, but village-level prioritization, building exposure assessment, and emergency planning require higher-resolution hazard and exposure data to avoid inflated or misleading exposure estimates.

6. Conclusions

This study evaluated the influence of spatial resolution on flood hazard simulation and exposure estimation in the downstream flood-prone region of the Upper Narmada Basin in India. HEC-RAS 2D simulations were performed at 30 × 30 m, 140 × 140 m, and 280 × 280 m resolutions and combined with building and population exposure data. The 30 × 30 m model agreed best with radar-derived flood extent, whereas the coarser models increasingly overestimated inundation. The overpredicted area increased from 51.30

https://doi.org/10.5194/egusphere-2026-4699
Preprint. Discussion started: 23 September 2026

km^2 at 30 m to 58.45 km^2 at 140 m and 73.36 km^2 at 280 m. This difference is mainly linked to terrain smoothing in coarse grids, which reduces the representation of narrow channels, local barriers, and floodplain connectivity. Resolution effects were also reflected in exposure estimates. The estimated number of affected buildings increased from 894 (2.5 times) at 30 m to 3051 (8.8 times) at 140 m and 11 537 (33 times) at 280 m, while affected population increased from 1612 to 5982 and 24 733, respectively. Coarse hazard and exposure layers can therefore inflate exposure estimates and exaggerate apparent village-level exposure hotspots. Spatial resolution is a key source of uncertainty in flood hazard and exposure assessment. Coarser models remain useful for broad regional screening, but village-level planning, building-specific exposure assessment, and emergency-response prioritization require hazard and exposure data at sufficiently fine resolution.

https://doi.org/10.5194/egusphere-2026-4699
Preprint. Discussion started: 23 September 2026

Data availability

Data can be provided by the corresponding author upon request.

Author contributions

PB: Conceptualization, Methodology, Data processing, Modelling output, Methodology and Formal analysis, Writing original draft preparation. NDN: Methodology, Writing (review and editing), Visualization. NV: Methodology, Writing (review and editing). LO: Provided exposure data HK: Supervision; Resources, Writing (review and editing). AA: Conceptualization, Methodology, Visualization, Supervision; Resources, Writing (review and editing).

Competing interests

Ankit Agarwal and Heidi Kreibich are members of the editorial board of Natural Hazards and Earth System Sciences.

Acknowledgements

The authors gratefully acknowledge the Digital Green Talent Award 2024 fellowship from Federal Ministry of Education and Research to conduct a research stay at Section: Hydrology, GFZ Helmholtz Centre for Geosciences and Indian Institute of Technology Roorkee for providing facilities to conduct PhD work. The authors also thank DK Ritushree, German Research Centre for Geosciences for supporting in the remote sensing data. AA acknowledge financial support from Department of science and Technology, Govt. of India under the BRICS framework DST/INT/BRICS/P-03/2024 (G).

Financial support:

No external funding was received for this research.

References

Alfieri, L., Burek, P., Dutra, E., Krzeminski, B., Muraro, D., Thielen, J., & Pappenberger, F. (2013). GloFAS – global ensemble streamflow forecasting and flood early warning. *Hydrology and Earth System Sciences*, *17*(3), 1161–1175. https://doi.org/10.5194/hess-17-1161-2013

Alfieri, L., Libertino, A., Campo, L., Dottori, F., Gabellani, S., Ghizzoni, T., Masoero, A., Rossi, L., Rudari, R., Testa, N., Trasforini, E., Amdihun, A., Ouma, J., Rossi, L., Tramblay, Y., Wu, H., & Massabò, M. (2023). *Impact-based flood forecasting in the Greater Horn of Africa* [Preprint]. Hydrological Hazards. https://doi.org/10.5194/egusphere-2023-804

Altenau, E. H., Pavelsky, T. M., Bates, P. D., & Neal, J. C. (2017). The effects of spatial resolution and dimensionality on modeling regional-scale hydraulics in a multichannel river. *Water Resources Research*, *53*(2), 1683–1701. https://doi.org/10.1002/2016WR019396

Arduino, G., Reggiani, P., & Todini, E. (2005). Recent advances in flood forecasting and flood risk assessment. *Hydrology and Earth System Sciences*, *9*(4), 280–284. https://doi.org/10.5194/hess-9-280-2005

Azizian, A., & Brocca, L. (2020). Determining the best remotely sensed DEM for flood inundation mapping in data sparse regions. *International Journal of Remote Sensing*, *41*(5), 1884–1906. https://doi.org/10.1080/01431161.2019.1677968

Badika, P., Raghuvanshi, A. S., & Agarwal, A. (2024). Climate change impact assessment on the hydrological response of the Tawa basin for sustainable water management. *Groundwater for Sustainable Development*, *26*, 101249. https://doi.org/10.1016/j.gsd.2024.101249

https://doi.org/10.5194/egusphere-2026-4699
Preprint. Discussion started: 23 September 2026

Bates, P. D. (2012). Integrating remote sensing data with flood inundation models: How far have we got? *Hydrological Processes*, *26*(16), 2515–2521. https://doi.org/10.1002/hyp.9374

Bhere, S., & Reddy, M. J. (2025). Flood risk assessment of suburban region in India by incorporating flood hazard, vulnerability and exposure. *Natural Hazards*, *121*(6), 6625–6649. https://doi.org/10.1007/s11069-024-07062-6

Bondarenko, M., Kerr, D., Sorichetta, A., & Tatem, A. (2020). *Census/projection-disaggregated gridded population datasets, adjusted to match the corresponding UNPD 2020 estimates, for 183 countries in 2020 using Built-Settlement Growth Model (BSGM) outputs* [Dataset]. University of Southampton. https://doi.org/10.5258/SOTON/WP00685

Brandt, S. A. (2016). Modeling and visualizing uncertainties of flood boundary delineation: Algorithm for slope and DEM resolution dependencies of 1D hydraulic models. *Stochastic Environmental Research and Risk Assessment*, *30*(6), 1677–1690. https://doi.org/10.1007/s00477-016-1212-z

Brussee, A. R., Bricker, J. D., De Bruijn, K. M., Verhoeven, G. F., Winsemius, H. C., & Jonkman, S. N. (2021). Impact of hydraulic model resolution and loss of life model modification on flood fatality risk estimation: Case study of the Bommelerwaard, The Netherlands. *Journal of Flood Risk Management*, *14*(3), e12713. https://doi.org/10.1111/jfr3.12713

Burn, D. H., & Whitfield, P. H. (2023). Climate related changes to flood regimes show an increasing rainfall influence. *Journal of Hydrology*, *617*, 129075. https://doi.org/10.1016/j.jhydrol.2023.129075

CWC. (2024). *Assessment of Area Affected Due to Floods in India (Part II: Assessment at Sub-District Level)*.

https://doi.org/10.5194/egusphere-2026-4699
Preprint. Discussion started: 23 September 2026

Dasgupta, A., Thakur, P. K., & Gupta, P. K. (2020). Potential of SAR-Derived Flood Maps for Hydrodynamic Model Calibration in Data Scarce Regions. *Journal of Hydrologic Engineering*, *25*(9), 05020028. https://doi.org/10.1061/(ASCE)HE.1943-5584.0001988

De Bruijn, K. M., & Klijn, F. (2009). Risky places in the Netherlands: A first approximation for floods. *Journal of Flood Risk Management*, *2*(1), 58–67. https://doi.org/10.1111/j.1753-318X.2009.01022.x

De Moel, H., & Aerts, J. C. J. H. (2011). Effect of uncertainty in land use, damage models and inundation depth on flood damage estimates. *Natural Hazards*, *58*(1), 407–425. https://doi.org/10.1007/s11069-010-9675-6

Fewtrell, T. J., Bates, P. D., Horritt, M., & Hunter, N. M. (2008). Evaluating the effect of scale in flood inundation modelling in urban environments. *Hydrological Processes*, *22*(26), 5107–5118. https://doi.org/10.1002/hyp.7148

Finkel, R. A., & Bentley, J. L. (1974). Quad trees a data structure for retrieval on composite keys. *Acta Informatica*, *4*(1), 1–9. https://doi.org/10.1007/BF00288933

Guimarães Nobre, G., De Moel, H., Giuliani, M., Bischiniotis, K., Aerts, J. C. J. H., & Ward, P. J. (2020). What Will the Weather Do? Forecasting Flood Losses Based on Oscillation Indices. *Earth's Future*, *8*(3), e2019EF001450. https://doi.org/10.1029/2019EF001450

Hooijer, A., Klijn, F., Pedroli, G. B. M., & Van Os, A. G. (2004). Towards sustainable flood risk management in the Rhine and Meuse river basins: Synopsis of the findings of IRMA-SPONGE. *River Research and Applications*, *20*(3), 343–357. https://doi.org/10.1002/rra.781

Huong, H. T. L., & Pathirana, A. (2013). Urbanization and climate change impacts on future urban flooding in Can Tho city, Vietnam. *Hydrology and Earth System Sciences*, *17*(1), 379–394. https://doi.org/10.5194/hess-17-379-2013

Intergovernmental Panel on Climate Change (IPCC). (2023). *Climate Change 2022 – Impacts, Adaptation and Vulnerability: Working Group II Contribution to the Sixth Assessment Report of the Intergovernmental Panel on Climate Change* (1st ed.). Cambridge University Press. https://doi.org/10.1017/9781009325844

Jiang, W., Yu, J., Wang, Q., & Yue, Q. (2022). Understanding the effects of digital elevation model resolution and building treatment for urban flood modelling. *Journal of Hydrology: Regional Studies*, *42*, 101122. https://doi.org/10.1016/j.ejrh.2022.101122

Jongman, B., Ward, P. J., & Aerts, J. C. J. H. (2012). Global exposure to river and coastal flooding: Long term trends and changes. *Global Environmental Change*, *22*(4), 823–835. https://doi.org/10.1016/j.gloenvcha.2012.07.004

Kiba, L. G., Nengzouzam, G., & Ranjan, P. (2023). Flood Hazard Mapping Using Hydraulic Models and GIS: A Review. In M. Pandey, A. K. Gupta, & G. Oliveto (Eds.), *River, Sediment and Hydrological Extremes: Causes, Impacts and Management* (pp. 65–72). Springer Nature Singapore. https://doi.org/10.1007/978-981-99-4811-6_4

Kimuli, J. B., Di, B., Zhang, R., Wu, S., Li, J., & Yin, W. (2021). A multisource trend analysis of floods in Asia-Pacific 1990–2018: Implications for climate change in sustainable development goals. *International Journal of Disaster Risk Reduction*, *59*, 102237. https://doi.org/10.1016/j.ijdrr.2021.102237

Kreibich, H., Di Baldassarre, G., Vorogushyn, S., Aerts, J. C. J. H., Apel, H., Aronica, G. T., Arnbjerg-Nielsen, K., Bouwer, L. M., Bubeck, P., Caloiero, T., Chinh, D. T., Cortès, M., Gain, A. K., Giampá, V., Kuhlicke, C., Kundzewicz, Z. W., Llasat, M. C., Mård, J.,

https://doi.org/10.5194/egusphere-2026-4699
Preprint. Discussion started: 23 September 2026

Matczak, P., … Merz, B. (2017). Adaptation to flood risk: Results of international paired flood event studies. *Earth's Future*, *5*(10), 953–965. https://doi.org/10.1002/2017EF000606

Kreibich, H., & Thieken, A. H. (2008). Assessment of damage caused by high groundwater inundation. *Water Resources Research*, *44*(9), 2007WR006621. https://doi.org/10.1029/2007WR006621

Lim, N. J., & Brandt, S. A. (2019). Flood map boundary sensitivity due to combined effects of DEM resolution and roughness in relation to model performance. *Geomatics, Natural Hazards and Risk*, *10*(1), 1613–1647. https://doi.org/10.1080/19475705.2019.1604573

Liu, Q., Du, M., Wang, Y., Deng, J., Yan, W., Qin, C., Liu, M., & Liu, J. (2024). Global, regional and national trends and impacts of natural floods, 1990–2022. *Bulletin of the World Health Organization*, *102*(06), 410–420. https://doi.org/10.2471/BLT.23.290243

Liu, Y., Bates, P., Neal, J. C., Slater, L., Zhao, J., & Ben-Haim, Z. (2025). A Bare-Earth GoogleDEM to Simulate Flooding in New Delhi, India. *Water Resources Research*, *61*(6), e2024WR038577. https://doi.org/10.1029/2024WR038577

Merz, B., Hall, J., Disse, M., & Schumann, A. (2010). Fluvial flood risk management in a changing world. *Natural Hazards and Earth System Sciences*, *10*(3), 509–527. https://doi.org/10.5194/nhess-10-509-2010

Nirupama, N., & Simonovic, S. P. (2007). Increase of Flood Risk due to Urbanisation: A Canadian Example. *Natural Hazards*, *40*(1), 25–41. https://doi.org/10.1007/s11069-006-0003-0

Nithila Devi, N., Ganapathy, A., Silva, A. F. R., Vorogushyn, S., Apel, H., Kreibich, H., Oostwegel, L. J. N., Kuiry, S. N., & Sairam, N. (2025). Lost water bodies and a flooded city – Counterfactual scenarios of the extreme Chennai flood highlight the potential of nature-based solutions. *Urban Climate*, *61*, 102454. https://doi.org/10.1016/j.uclim.2025.102454

Olang, L. O., & Fürst, J. (2011). Effects of land cover change on flood peak discharges and runoff volumes: Model estimates for the Nyando River Basin, Kenya. *Hydrological Processes*, *25*(1), 80–89. https://doi.org/10.1002/hyp.7821

Ongdas, N., Akiyanova, F., Karakulov, Y., Muratbayeva, A., & Zinabdin, N. (2020). Application of HEC-RAS (2D) for Flood Hazard Maps Generation for Yesil (Ishim) River in Kazakhstan. *Water*, *12*(10), 2672. https://doi.org/10.3390/w12102672

Pandidurai, D., Raghuvanshi, A. S., Agarwal, A., & Trigo, R. M. (2026). Sequential Moisture Dynamics Driving Multi-Day Flood-Producing Rainfall Across India. *International Journal of Climatology*, e70462. https://doi.org/10.1002/joc.70462

Pappenberger, F., Dutra, E., Wetterhall, F., & Cloke, H. L. (2012). Deriving global flood hazard maps of fluvial floods through a physical model cascade. *Hydrology and Earth System Sciences*, *16*(11), 4143–4156. https://doi.org/10.5194/hess-16-4143-2012

Petrow, T., Thieken, A. H., Kreibich, H., Merz, B., & Bahlburg, C. H. (2006). Improvements on Flood Alleviation in Germany: Lessons Learned from the Elbe Flood in August 2002. *Environmental Management*, *38*(5), 717–732. https://doi.org/10.1007/s00267-005-6291-4

Rathod, P., & Manekar, V. L. (2020). Parameter Uncertainty in HEC-RAS 1D CSU Scour Model. *Current Science*, *118*(8), 1227. https://doi.org/10.18520/cs/v118/i8/1227-1234

https://doi.org/10.5194/egusphere-2026-4699
Preprint. Discussion started: 23 September 2026

Saksena, S., & Merwade, V. (2015). Incorporating the effect of DEM resolution and accuracy for improved flood inundation mapping. *Journal of Hydrology*, *530*, 180–194. https://doi.org/10.1016/j.jhydrol.2015.09.069

Savage, J. T. S., Bates, P., Freer, J., Neal, J., & Aronica, G. (2016). When does spatial resolution become spurious in probabilistic flood inundation predictions? *Hydrological Processes*, *30*(13), 2014–2032. https://doi.org/10.1002/hyp.10749

Schorlemmer, D., Oostwegel, L. J. N., Lingner, L., & Evaz Zadeh, T. (2024). *A model of European buildings* (Version 23/07) [Dataset]. GFZ Data Services. https://doi.org/10.5880/GFZ.2.6.2023.011

Schwanghart, W., Agarwal, A., Cook, K., Ozturk, U., Shukla, R., & Fuchs, S. (2024). Preface: Estimating and predicting natural hazards and vulnerabilities in the Himalayan region. *Natural Hazards and Earth System Sciences*, *24*(9), 3291–3297. https://doi.org/10.5194/nhess-24-3291-2024

Sharma, V. C., & Regonda, S. K. (2021a). Two-Dimensional Flood Inundation Modeling in the Godavari River Basin, India—Insights on Model Output Uncertainty. *Water*, *13*(2), 191. https://doi.org/10.3390/w13020191

Sharma, V. C., & Regonda, S. K. (2021b). Two-Dimensional Flood Inundation Modeling in the Godavari River Basin, India—Insights on Model Output Uncertainty. *Water*, *13*(2), 191. https://doi.org/10.3390/w13020191

Sirko, W., Kashubin, S., Ritter, M., Annkah, A., Bouchareb, Y. S. E., Dauphin, Y., Keysers, D., Neumann, M., Cisse, M., & Quinn, J. (2021). *Continental-Scale Building Detection from High Resolution Satellite Imagery* (arXiv:2107.12283). arXiv. https://doi.org/10.48550/arXiv.2107.12283

Staffler, H., Pollinger, R., Zischg, A., & Mani, P. (2008). Spatial variability and potential impacts of climate change on flood and debris flow hazard zone mapping and

https://doi.org/10.5194/egusphere-2026-4699
Preprint. Discussion started: 23 September 2026

implications for risk management. *Natural Hazards and Earth System Sciences*, *8*(3), 539–558. https://doi.org/10.5194/nhess-8-539-2008

Teng, J., Jakeman, A. J., Vaze, J., Croke, B. F. W., Dutta, D., & Kim, S. (2017). Flood inundation modelling: A review of methods, recent advances and uncertainty analysis. *Environmental Modelling & Software*, *90*, 201–216. https://doi.org/10.1016/j.envsoft.2017.01.006

Vashist, K., & Singh, K. K. (2023). HEC-RAS 2D modeling for flood inundation mapping: A case study of the Krishna River Basin. *Water Practice & Technology*, *18*(4), 831–844. https://doi.org/10.2166/wpt.2023.048

Vashistha, A., Joshi, S., & Siva Subramanian, S. (2025). Scenario-based probabilistic risk assessment of earthquake-induced landslides in Uttarakhand, India. *Stochastic Environmental Research and Risk Assessment*, *39*(11), 5049–5069. https://doi.org/10.1007/s00477-025-03067-0

Vogel, R. M., Yaindl, C., & Walter, M. (2011). Nonstationarity: Flood Magnification and Recurrence Reduction Factors in the United States1: Nonstationarity: Flood Magnification and Recurrence Reduction Factors in the United States. *JAWRA Journal of the American Water Resources Association*, *47*(3), 464–474. https://doi.org/10.1111/j.1752-1688.2011.00541.x

Wasko, C., Nathan, R., Stein, L., & O'Shea, D. (2021). Evidence of shorter more extreme rainfalls and increased flood variability under climate change. *Journal of Hydrology*, *603*, 126994. https://doi.org/10.1016/j.jhydrol.2021.126994

Wasko, C., & Sharma, A. (2017). Global assessment of flood and storm extremes with increased temperatures. *Scientific Reports*, *7*(1), 7945. https://doi.org/10.1038/s41598-017-08481-1

https://doi.org/10.5194/egusphere-2026-4699
Preprint. Discussion started: 23 September 2026

Williams, S., Griffiths, J., Miville, B., Romeo, E., Leiofi, M., O'Driscoll, M., Iakopo, M., Mulitalo, S., Ting, J. C., Paulik, R., & Elley, G. (2021). An Impacts-Based Flood Decision Support System for a Tropical Pacific Island Catchment with Short Warnings Lead Time. *Water*, *13*(23), 3371. https://doi.org/10.3390/w13233371

Yu, D., & Lane, S. N. (2006). Urban fluvial flood modelling using a two-dimensional diffusion-wave treatment, part 1: Mesh resolution effects. *Hydrological Processes*, *20*(7), 1541–1565. https://doi.org/10.1002/hyp.5935

Zischg, A. P., Mosimann, M., Bernet, D. B., & Röthlisberger, V. (2018). Validation of 2D flood models with insurance claims. *Journal of Hydrology*, *557*, 350–361. https://doi.org/10.1016/j.jhydrol.2017.12.042